The Journal of Immunology

Mouse Cytomegalovirus Infection in BALB/c Mice Resembles Virus-Associated Secondary Hemophagocytic Lymphohistiocytosis and Shows a Pathogenesis Distinct from Primary Hemophagocytic Lymphohistiocytosis

Ellen Brisse, Maya Imbrechts, Karen Put, Anneleen Avau, Tania Mitera, Nele Berghmans, Omer Rutgeerts, Mark Waer, Marisa Ninivaggi, Hilde Kelchtermans, Louis Boon, Robert Snoeck, Carine H. Wouters, Graciela Andrei and Patrick Matthys

J Immunol 2016; 196:3124-3134; Prepublished online 22 February 2016;
doi: 10.4049/jimmunol.1501035
http://www.jimmunol.org/content/196/7/3124

The Journal of Immunology is published twice each month by
The American Association of Immunologists, Inc.,
9650 Rockville Pike, Bethesda, MD 20814-3994.

Print ISSN: 0022-1767 Online ISSN: 1550-6606.

Mouse Cytomegalovirus Infection in BALB/c Mice Resembles Virus-Associated Secondary Hemophagocytic Lymphohistiocytosis and Shows a Pathogenesis Distinct from Primary Hemophagocytic Lymphohistiocytosis

Ellen Brisse,* Maya Imbrechts,* Karen Put,* Anneleen Avau,* Tania Mitera,* Nele Berghmans,† Omer Rutgeerts,‡ Mark Waer,‡ Marisa Ninivaggi,§ Hilde Kelchtermans,§ Louis Boon,¶ Robert Snoeck,‖ Carine H. Wouters,# Graciela Andrei,‖ and Patrick Matthys*

Hemophagocytic lymphohistiocytosis (HLH) is a life-threatening immunological disorder that is characterized by systemic inflammation, widespread organ damage, and hypercytokinemia. Primary HLH is caused by mutations in granule-mediated cytotoxicity, whereas secondary HLH occurs, without a known genetic background, in a context of infections, malignancies, or autoimmune and autoinflammatory disorders. Clinical manifestations of both HLH subtypes are often precipitated by a viral infection, predominantly with *Herpesviridae*. Exploiting this knowledge, we established an animal model of virus-associated secondary HLH by infecting immunocompetent wild-type mice with the β-herpesvirus murine CMV. C57BL/6 mice developed a mild inflammatory phenotype, whereas BALB/c mice displayed the clinicopathologic features of HLH, as set forth in the Histiocyte Society diagnostic guidelines: fever, cytopenia, hemophagocytosis, hyperferritinemia, and elevated serum levels of soluble CD25. BALB/c mice also developed lymphadenopathy, liver dysfunction, and decreased NK cell numbers. Lymphoid and myeloid cells were in a hyperactivated state. Nonetheless, depletion of $CD8^+$ T cells could not inhibit or cure the HLH-like syndrome, highlighting a first dissimilarity from mouse models of primary HLH. Immune cell hyperactivation in BALB/c mice was accompanied by a cytokine storm. Notably, plasma levels of IFN-γ, a key pathogenic cytokine in models of primary HLH, were the highest. Nevertheless, murine CMV–infected IFN-γ–deficient mice still developed the aforementioned HLH-like symptoms. In fact, IFN-γ–deficient mice displayed a more complete spectrum of HLH, including splenomegaly, coagulopathy, and decreased NK cell cytotoxicity, indicating a regulatory role for IFN-γ in the pathogenesis of virus-associated secondary HLH as opposed to its central pathogenic role in primary HLH. ***The Journal of Immunology*****, 2016, 196: 3124–3134.**

Hemophagocytic lymphohistiocytosis (HLH) is a rare, but increasingly recognized, hyperinflammatory syndrome that is characterized by an uncontrolled activation of macrophages and lymphocytes and a life-threatening cytokine storm, eliciting hallmark features such as nonremitting fever, pancytopenia, coagulopathy, hyperferritinemia, hemophagocytosis, and liver dysfunction. HLH can be subdivided into primary and secondary forms. Although the former has a monogenic recessive inheritance, being caused by mutations in genes that regulate granule-dependent cytotoxicity of cytotoxic T cells and NK cells, the latter occurs without a distinct genetic background as a complication of various malignancies, infections, or autoimmune and autoinflammatory diseases (1, 2).

With regard to primary HLH, considerable progress has been made in deciphering its pathogenesis, largely by studying mouse strains that carry similar mutations as those occurring in the different subtypes of primary HLH (3–9). In HLH disease models using these mouse strains, hyperactivated $CD8^+$ T cells, producing large amounts of IFN-γ, were pinpointed as major pathogenic players. Depletion of this cell type, as well as ablation of IFN-γ, was associated with significantly reduced disease severity (4, 10). Moreover, infusion of a physiologically relevant dose of IFN-γ provoked profound cytopenias and hemophagocytosis in mice (11), possibly explaining the occurrence of these cardinal features in HLH patients. Together, these data constitute the rationale for an ongoing clinical trial in which patients with refractory primary HLH receive treatment with a human monoclonal anti–IFN-γ Ab (EudraCT: 2012-003632-23, US NCT: NCT01818492).

Knowledge about secondary HLH has evolved less rapidly. Hypotheses concerning its pathogenesis, including a key role for

*Laboratory of Immunobiology, Rega Institute, University of Leuven, 3000 Leuven, Belgium; †Laboratory of Molecular Immunology, Rega Institute, University of Leuven, 3000 Leuven, Belgium; ‡Laboratory of Experimental Transplantation, University of Leuven, 3000 Leuven, Belgium; §Synapse BV, Cardiovascular Research Institute Maastricht School for Cardiovascular Diseases, Maastricht University, 6229 Maastricht, the Netherlands; ¶Epirus Biopharmaceuticals Netherlands, 3584 Utrecht, the Netherlands; ‖Laboratory of Virology and Chemotherapy, Rega Institute, University of Leuven, 3000 Leuven, Belgium; and #Laboratory of Pediatric Immunology, University Hospital Gasthuisberg, University of Leuven, 3000 Leuven, Belgium

Received for publication May 4, 2015. Accepted for publication January 22, 2016.

This work was supported by grants from the Agency for Innovation by Science and Technology, the Research Foundation Flanders, the Regional Government of Flanders (Concerted Research Actions program), and the Interuniversity Attraction Poles. E.B. received a fellowship from the Agency for Innovation by Science and Technology. K.P. and A.A. received fellowships from the Research Foundation Flanders.

Address correspondence and reprint requests to Dr. Patrick Matthys, Laboratory of Immunobiology, Rega Institute, University of Leuven, Minderbroedersstraat 10, 3000 Leuven, Belgium. E-mail address: patrick.matthys@kuleuven.be

The online version of this article contains supplemental material.

Abbreviations used in this article: ALT, alanine transaminase; AST, aspartate transaminase; FSC, forward scatter; HLH, hemophagocytic lymphohistiocytosis; KO, knockout; LN, lymph node; MCMV, murine CMV; MFI, mean fluorescence intensity; MHCI, MHC class I; MHCII, MHC class II; p.i., postinfection; PI, propidium iodide; sCD25, soluble CD25; SSC, side scatter; T_{EM}, effector memory T cell; WT, wild-type.

www.jimmunol.org/cgi/doi/10.4049/jimmunol.1501035

IFN-γ and hyperactivated $CD8^+$ T cells, are largely inspired by the findings in mouse models of primary HLH. Although some animal models have been proposed for secondary HLH (12–17), few specifically addressed the possible pathogenic role of IFN-γ or $CD8^+$ T cells (14, 18). Those that did revealed an ambiguous role for IFN-γ in disease development (14, 18), whereas $CD8^+$ T cells were dispensable for disease pathogenesis (14). These data suggest a possible discrepancy between primary and secondary HLH and highlight the need for further research on differential pathogenic mechanisms in both HLH subtypes (19).

Because secondary HLH in humans can occur without a distinct underlying genetic predisposition and is often precipitated by a viral infection, predominantly with EBV or CMV (20–23), we investigated whether HLH-like disease might, under certain circumstances, develop in immunocompetent, wild-type (WT) mice postinfection (p.i.) with the β-herpesvirus murine CMV (MCMV).

MCMV was used in models of primary HLH, where it successfully elicits HLH in *Prf1*-knockout (KO) mice but not in *Unc13d*-KO mice (7, 24). The genetic background of different inbred mouse strains plays a role in susceptibility to MCMV. C57BL/6 mice are relatively resistant to the virus and often remain asymptomatic p.i., whereas BALB/c mice are more sensitive. Unlike C57BL/6 mice, BALB/c mice lack the NK cell–activating receptor Ly49H that specifically recognizes m157, an MHC class I (MHCI)-like protein expressed by MCMV (25). Instead, an inhibitory receptor, Ly49C, might recognize the protein, mediating viral immune evasion (26). This minor NK cell defect hinders efficient recognition and clearance of the virus, resulting in prolonged immune activation.

In this article, we demonstrate that a fine-tuned experimental infection with MCMV reproducibly induced an HLH-like syndrome in WT BALB/c mice compared with mild and transient inflammatory signs in WT C57BL/6 mice. $CD8^+$ T cells were dispensable for the development of the syndrome in BALB/c mice. By comparing disease features in WT and IFN-γ–deficient BALB/c mice, we also showed that IFN-γ did not drive disease pathogenesis, but rather acted in a protective manner by increasing survival, attenuating symptoms, preventing the development of coagulation abnormalities, and tempering the amplification of the cytokine storm p.i. The data suggest that the pathogenesis of virus-associated secondary HLH is different from that of primary HLH, which cautions against the extrapolation of treatment strategies from primary HLH to the secondary subtypes.

Materials and Methods

Mice, viral infection, and experimental design

The generation and characterization of IFN-γ–KO mice were described previously (27). IFN-γ–KO mice on a BALB/c background, corresponding WT BALB/c mice, and WT C57BL/6 mice were bred under specific pathogen–free conditions in the Experimental Animal Centre of the University of Leuven. Four- to six-week-old mice were matched for age and sex within each experiment. All experiments were approved by the Ethics Committee of the University of Leuven. An inoculum of 5×10^3 PFU salivary gland–derived MCMV (Smith strain, VR-1399; American Type Culture Collection) in 100 μl PBS was injected i.p. into each mouse on day 0. PBS-injected mice were included as controls. Weight and rectal temperature of the mice were measured daily. Mice were euthanized with pentobarbital (Nembutal; Ceva) on day 2 p.i., at the first signs of inflammation, or on day 5 p.i., according to institutional ethical policies, when chronic weight loss exceeded 25% of initial body weight or when body temperature dropped below 34.5°C.

Quantification of viral titers and T cell depletion

The amount of infectious virus present in different organs was determined by a plaque assay using a 10-fold titration of the supernatant of disrupted organ samples on C127I cells (CRL-1616; American Type Culture Collection).

To deplete $CD8^+$ T cells, a monoclonal anti-CD8 Ab (clone YTS169) was injected i.p. as a preventive treatment (300 μg/mouse on day −1 and 200 μg/mouse on day 2 p.i., in 100 μl PBS) or a curative treatment (300 μg/mouse in 100 μl PBS on day 2 p.i.). Depletion was verified in blood and lymph nodes (LN) via flow cytometry using anti-CD8a (clone 53-6.7).

Blood analysis, quantification of liver enzymes, and thrombin generation

Blood samples were obtained via cardiac puncture with heparin (LEO Pharma). Blood cell analysis was performed with a Cell-Dyn 3700 Hematology Analyzer (Abbott Diagnostics). Plasma concentrations of aspartate transaminase (AST) and alanine transaminase (ALT) were measured spectrophotometrically using a UV-kinetic method, according to the manufacturer's instructions (ALT [SGPT] Reagent Set, AST [SGOT] Reagent Set; Teco Diagnostics). A Calibrated Automated Thrombogram assay measuring thrombin generation over time was performed in collaboration with Synapse BV on whole blood drawn via retro-orbital puncture, as described previously (28). Samples were measured in triplicate.

Histology, single-cell suspensions, cytospins, and flow cytometry

For histological analysis, tissues fixed in 4% paraformaldehyde were embedded in paraffin. Sections were stained with H&E. For single-cell suspensions, WBC were obtained from blood after lysis of RBC with NH_4Cl. Bone marrow was extracted from the tibia of both hind legs. Lung WBC were obtained from density gradient–centrifuged lung cell suspensions (Percoll 40 and 72%; GE Healthcare). Splenocytes were obtained after RBC lysis with ACK Lysing Buffer (Life Technologies). Lymph node cells were extracted from both inguinal LN. For cytospin preparations, single-cell suspensions were spun onto a glass slide and stained with H&E. For flow cytometry, cell suspensions were incubated with anti-CD16/anti-CD32 (Miltenyi Biotec) and stained with the following mAb: CD3e (clone 145-2C11), CD8a (53-6.7), CD11b (M1/70), CD25 (PC61.5), CD44 (IM7), CD49b (DX5), CD62L (MEL-14), CD69 (H1.2F3), CD80 (16.10A1), CD86 (GL1), CD107a (eBio1D4B), CD122 (5H4), MHCI (28.14-8), and MHC class II (MHCII) I-A/I-E (M5/114.15.2) (eBioscience). FITC-, PE-, PE-Cy5–, PerCP-Cy5.5–, or allophycocyanin-labeled Abs were used. Dead cells were excluded using propidium iodide (PI). Geometric means were used to calculate mean fluorescence intensity (MFI). Forward scatter (FSC) was used to measure cell size, and side scatter (SSC) was used to measure granularity. Samples were run with a FACSCalibur using CellQuest software (BD Biosciences). Live cells (PI^-) were analyzed with FlowLogic (600.0A; Inivai).

Cell-mediated cytotoxicity assay and NK cell enrichment

A [^{51}Cr]-release assay was performed in triplicate, as described previously (29). The YAC-1 cell line was used as target cells. Effector cells were WBC isolated from blood samples, lung WBC, or NK cells enriched from lung or spleen WBC via MACS using magnetic beads coated with anti-CD49b (DX5) mAb (Miltenyi Biotec). E:T ratios of 25:1 and 50:1 were assessed.

Quantification of cytokine expression using quantitative real-time PCR

Total RNA was extracted using a PureLink RNA Mini Kit (Invitrogen). cDNA was synthetized using Superscript II reverse transcriptase and random primers (Invitrogen). Quantitative real-time PCR was performed using a TaqMan Gene Expression Assay (Applied Biosystems). Expression levels of *Il1b* (assay ID Mm00434228_m1), *Il6* (Mm00446190_m1), *Il10* (Mm00439614_m1), *Il18* (Mm00434225_m1), *Il18bp* (Mm01274147_g1), *Ifng* (Mm00801778_m1), and *Tnfa* (Mm00443258_m1) were normalized to the expression of *Gapdh* (Mm99999915_g1). Relative gene expression was calculated using the $2^{-\Delta\Delta Ct}$ method (30).

Quantification of cytokines, soluble CD25, ferritin, and D-dimers using ELISA

The protein levels of IFN-α, IFN-β (VeriKine; PBL IFN Source), IL-1β, TNF-α, soluble CD25 (sCD25) (DuoSet; R&D Systems), IL-6, IL-10 (Quantikine; R&D Systems), IFN-γ (Ready-Set-Go; eBioscience), IL-18 (Platinum ELISA; eBioscience), and D-dimers (D2D, TSZ ELISA; BioTang) were determined in plasma, according to the manufacturers' instructions. Alternatively, IFN-α, IFN-β, IFN-γ, IL-1β, IL-2, IL-6, IL-10, IL-12p70, IL-18, and TNF-α were measured in serum using a multiplex assay (ProcartaPlex Mouse Th1/Th2 Cytokine Panel, Th9/Th17/Th22/Treg

Cytokine Panel, or IFN-α/IFN-β Panel; eBioscience). Sandwich ELISA detecting the H and L chain of ferritin were kindly provided by Dr. Paolo Santambrogio (San Raffaele Scientific Institute, Il Dipartimento di Biotecnologie, Milan, Italy) (31).

Statistical analysis

Data with two experimental groups were analyzed via a two-tailed nonparametric Mann–Whitney *U* test. For comparison of three or more groups, a nonparametric Kruskal–Wallis test was performed, followed by the Dunn multiple–comparison posttest. GraphPad Prism 5.00 was used.

Results

Acute, primary infection with MCMV triggers a severe HLH-like syndrome in WT BALB/c mice

From pilot experiments in which mice were infected with titers ranging from 2.5×10^3 to 1×10^5 PFU of MCMV, a dose of 5×10^3 PFU was selected as the lowest dose of MCMV from which mice developed clinical signs of illness within an appropriate time frame and within the ethical constraints of our institute. In C57BL/6 mice, the infection resulted in transient signs of a mild inflammatory response. However, in BALB/c mice, the infection caused a life-threatening, hyperinflammatory syndrome that was highly reminiscent of the HLH syndrome observed in patients. To thoroughly characterize this syndrome, we applied the HLH-2004 criteria that are used in the clinical setting to diagnose HLH, consisting of eight components: fever, splenomegaly, cytopenia affecting at least two blood cell lineages, hypofibrinogenemia and/or hypertriglyceridemia, hemophagocytosis, decreased NK cell activity, hyperferritinemia, and elevated serum levels of sCD25. At least five criteria need to be fulfilled to diagnose HLH in patients (32).

Starting on day 2 p.i., BALB/c and C57BL/6 mice became ill, as evident from piloerection and weight loss. The latter was significantly more pronounced in BALB/c mice (Fig. 1A, Supplemental Fig. 1A). The body temperature of both mouse strains increased, but only BALB/c mice developed a marked fever, rising above 38.5˚C (Fig. 1B, Supplemental Fig. 1D). The fever gradually evolved to hypothermia (<34.5˚C) on day 5 p.i. in ~40% of the BALB/c mice (Fig. 1C), necessitating euthanasia. In contrast, all infected C57BL/6 mice recovered from infection, regaining their original weight. The virus could be efficiently cleared by C57BL/6 mice, as evidenced by undetectable or low viral titers in spleen at days 2 and 5 p.i., whereas persistently high viral titers were detected in infected BALB/c mice (Supplemental Fig. 1B, 1C).

Blood analysis on day 5 p.i. revealed bicytopenia in infected BALB/c mice. Lymphopenia and thrombocytopenia were observed in all experiments performed (Fig. 1D, 1E), whereas additional anemia occurred in 70% of the experiments (Fig. 1F). The cytopenias could result, in part, from decreased blood cell production, as indicated by minor bone marrow hypocellularity on day 5 p.i. (Fig. 1G). Infected C57BL/6 mice did not develop significant cytopenias, although a trend was observed (Supplemental Fig. 1E–G). Hemophagocytosis was detected in infected BALB/c mice from day 2 p.i. (data not shown) and was abundant on day 5 p.i. in blood, lung, and bone marrow (Fig. 1H, 1I). Hemophagocytes were also observed in infected C57BL/6 mice, but their numbers were not significantly different from those of naive C57BL/6 mice (Supplemental Fig. 1H). Plasma levels of ferritin and sCD25 were increased in infected BALB/c mice (Fig. 1J, 1K) to greater concentrations than seen in infected C57BL/6 mice (Supplemental Fig. 1I, 1J). Both H chain (Fig. 1J) and L chain (data not shown) ferritin levels were consistently upregulated, although the levels varied between independent experiments, ranging from 100 to 4400 ng/ml.

In contrast to the human HLH syndrome, MCMV-infected BALB/c mice developed neutrophilia instead of neutropenia (data not shown), a phenomenon that was also reported in other mouse models of HLH (7, 12, 33). Furthermore, measurements of serum triglycerides and fibrinogen revealed no hypertriglyceridemia or hypofibrinogenemia in infected BALB/c mice (data not shown). In patients, these symptoms reflect, in part, the involvement of liver inflammation in the HLH syndrome, of which significant signs were detected in MCMV-infected BALB/c mice. Histological examination of liver tissue revealed perivascular infiltration of immune cells (Fig. 2A) and significantly elevated plasma levels of ALT (Fig. 2B) and AST (data not shown), which are often used as biomarkers for hepatocellular damage (34). Immune cell infiltration was also observed in the spleen of infected BALB/c mice, together with the disappearance of distinct red and white pulpa, indicating disruption of the normal spleen architecture (Fig. 2C). This might explain the lack of splenomegaly. Infected BALB/c mice displayed signs of lymphoproliferation, as manifested by the enlargement of the inguinal LN (Fig. 2D). This lymphadenopathy can likely be attributed to a combination of edema, hyperplasia, and hypertrophy of LN cells (Fig. 2E, 2F).

Patients with primary HLH characteristically possess pronounced defects in NK cell cytotoxicity, as does a variable percentage of patients with secondary HLH (35–37). To investigate NK cell function in the model, [^{51}Cr]-release assays were performed on enriched lung NK cells, as well as on the total WBC fraction of lungs. Neither revealed defects; on the contrary, the cytotoxic function of MCMV-infected BALB/c mice was markedly increased in comparison with that of naive counterparts (Fig. 2G, 2H). An intact cytotoxic function was confirmed for NK cells extracted from spleen, blood, and lungs via detection of CD107a surface expression. CD107a is a lysosome-associated membrane protein present inside cytotoxic granules that, upon degranulation, appears on the cell surface of cytotoxic cells (35, 38). CD107a expression on enriched splenic NK cells (Fig. 2I) and NK cells extracted from blood or lungs (data not shown) was increased in MCMV-infected BALB/c mice, indicating increased degranulation. The cytotoxic function of infected C57BL/6 mice was comparable to that of BALB/c mice (Supplemental Fig. 1K). In addition to functional defects, peripheral blood NK cell numbers are also frequently reduced during active disease in secondary HLH patients (2, 39, 40). In BALB/c mice, the percentage and absolute number of NK cells declined sharply in lungs, blood, and spleen upon infection (Fig. 2J, 2K, data not shown), whereas the NK cell numbers of infected C57BL/6 mice were not affected or were slightly elevated (Supplemental Fig. 1L, 1M).

In brief, WT BALB/c mice developed an acute, life-threatening syndrome that reflected several keynote features of HLH and fulfilled five of eight HLH-2004 criteria, after primary infection with a naturally occurring murine herpesvirus. In contrast, infected WT C57BL/6 mice displayed a transient and controlled inflammatory response that did not culminate in an HLH-like syndrome.

Immune cell hyperactivation and hypercytokinemia underlie the HLH-like syndrome in MCMV-infected WT BALB/c mice

Many characteristic symptoms of HLH can be attributed to aberrant activation of cytotoxic T cells, ongoing Ag presentation by APC, and a severe cytokine storm (1, 41–43). In MCMV-infected BALB/c mice, these hallmark features of HLH were also observed. Activation of T cells and macrophages was already presumed from the increased levels of sCD25 and ferritin in plasma (44–46). Indeed, CD8$^+$ T cells extracted from spleen, LN, lungs, and blood showed an activated profile when examining very early (CD69) and intermediate early (CD25) activation markers (47, 48). Increased

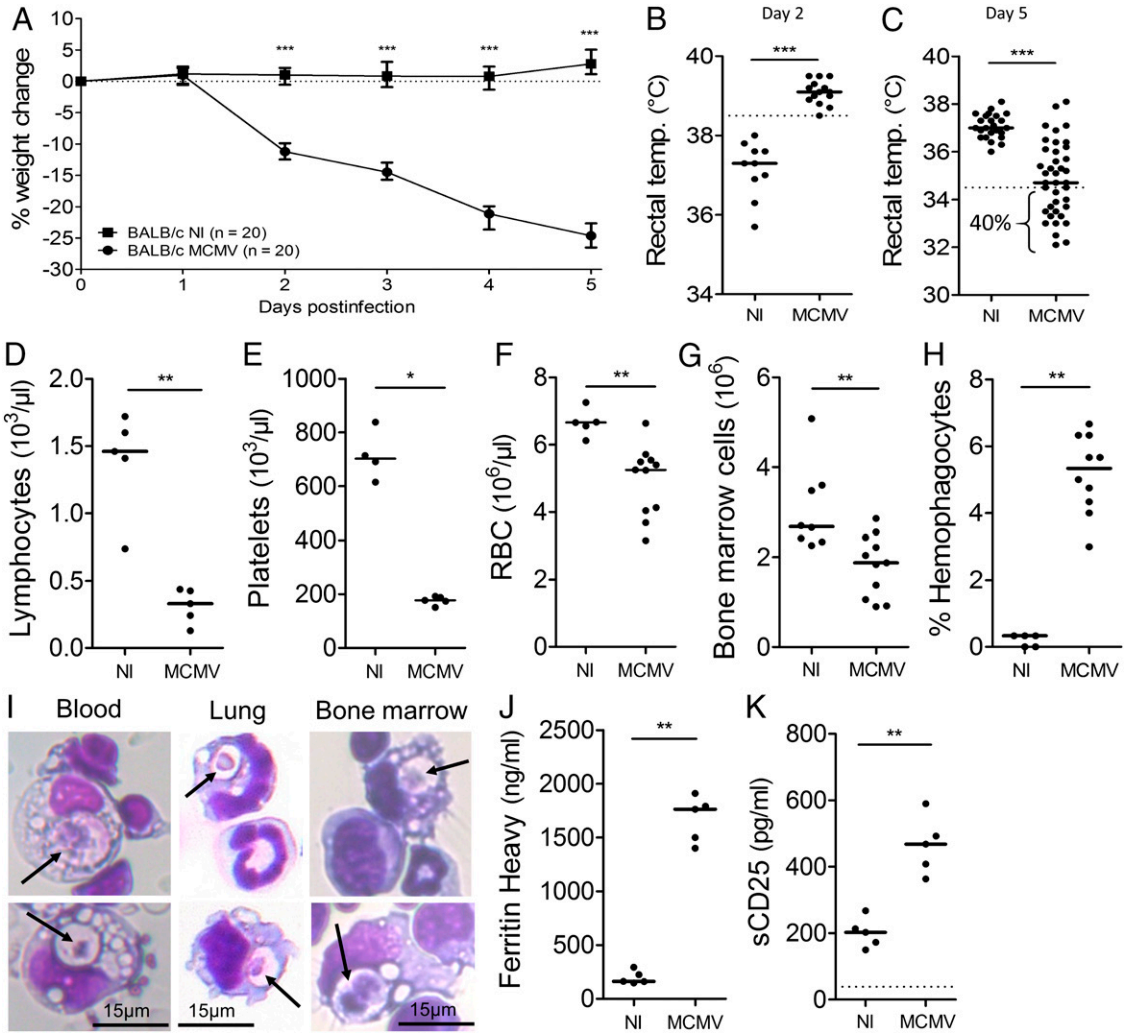

FIGURE 1. HLH-2004 criteria assessed in WT BALB/c mice infected with 5×10^3 PFU of MCMV. (**A**) Percentage change in body weight relative to initial body weight at day 0 p.i. Median with interquartile range of 20 mice/experimental group. Rectal body temperature (˚C) on day 2 (**B**) and day 5 (**C**) p.i. Dotted line = 38.5˚C (fever) or 34.5˚C (endpoint as an indication of mortality). Absolute lymphocyte (**D**), platelet (**E**), and RBC (**F**) counts in whole blood at day 5 p.i. (**G**). Total bone marrow cell number at day 5 p.i. (**H**) Percentage of hemophagocytes detected in cytospins of bone marrow cells at day 5 p.i. Dots represent the average of triplicate counts of 100 cells from an individual mouse. (**I**) Hemophagocytes detected in cytospins from blood, lung, and bone marrow cells of MCMV-infected BALB/c mice on day 5 p.i. (H&E). Engulfed cells are indicated by arrows. (**J**) Concentration of the ferritin H chain in plasma (ng/ml) at day 5 p.i. Dots represent the average of two dilutions for a single mouse. (**K**) Concentration of sCD25 in plasma (pg/ml) at day 5 p.i. Dotted line in (K) represents the ELISA lower detection limit. Dots in (B)–(G) and (K) represent individual animals. Horizontal lines represent median group values. Depicted data are from one to five experiments and are representative of 3 to ≥10 independent experiments with at least four mice/experimental group. $*p < 0.05$, $**p < 0.01$, $***p < 0.001$, Mann–Whitney *U* test. NI, not infected; temp., temperature.

proportions of $CD8^+$ T cells stained positive for CD69 and CD25, and the expression intensity of CD25/individual cell was augmented (Fig. 3A, 3B). The expression intensity of CD69 on splenic $CD8^+$ T cells varied (decreased, unchanged, or increased) throughout different experiments (Fig. 3A), but it was consistently increased on LN, lung, and blood $CD8^+$ T cells, indicating organ-specific differences in the timing of immune cell activation (data not shown). Upon activation, shedding of CD62L (L-selectin), together with upregulation of CD44, separates the $CD8^+$ T cell population into naive T cells ($CD62L^+CD44^-$), central memory T cells ($CD62L^+CD44^+$), and effector memory T cells (T_{EM}; $CD62L^-CD44^+$) (49). Postinfection with MCMV, a marked shift from naive $CD8^+$ T cells into differentiated T_{EM} was seen in spleen (Fig. 3C) and LN (data not shown). This activation status was reflected by enlargement of the $CD8^+$ T cell size and increased granularity (Fig. 3D). Notably, the activation level of $CD8^+$ T cells in infected BALB/c mice was substantially higher compared with $CD8^+$ T cells of infected C57BL/6 mice (Supplemental Fig. 2A, 2B, 2E).

Extensive activation of histiocytes was detected in the spleen and LN of MCMV-infected BALB/c mice (Fig. 3, data not shown). Large $CD11b^{high}$-expressing cells (Fig. 3E), a fraction containing predominantly macrophages, monocyte-derived dendritic cells, and neutrophils, displayed an activated phenotype with upregulation of CD80 and CD86 (Fig. 3F, 3G), two costimulatory molecules required for the initiation and maintenance of T cell activation and proliferation (50). These large $CD11b^{high}$ cells were additionally increased in cell size and granularity upon infection (Fig. 3H). Consistent with the flow cytometry data, cytospins from splenocytes of infected mice revealed the presence of histiocytes displaying extensive vacuolization (Fig. 3I). In line with their importance as primary sites of Ag presentation, LN-derived large $CD11b^{high}$ cells augmented their expression of MHCII (Fig. 3J). Together with an overall increase in MHCI expression in spleen and

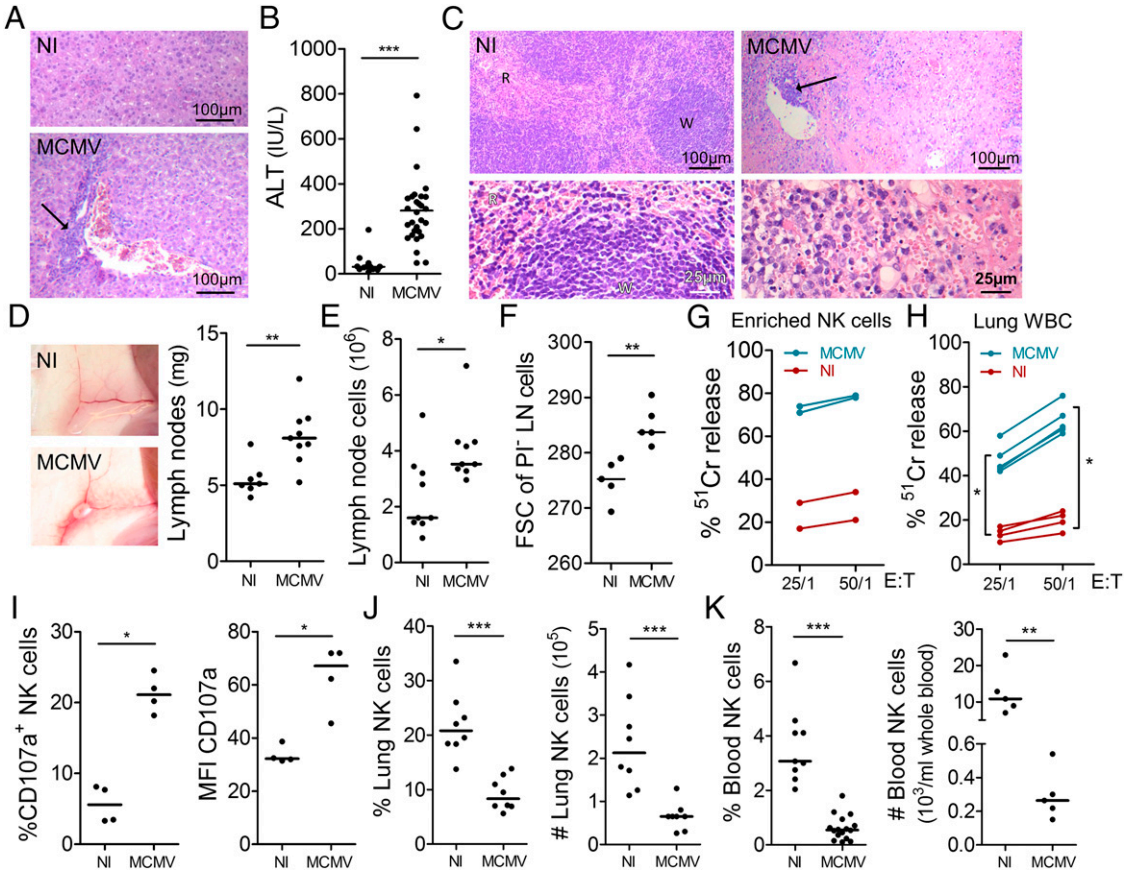

FIGURE 2. Additional HLH-like features assessed in WT BALB/c mice infected with 5×10^3 PFU of MCMV. (**A**) Liver histology of H&E-stained paraffin sections. Arrow indicates perivascular infiltration. (**B**) Plasma concentration of ALT (IU/l). (**C**) Spleen histology of H&E-stained paraffin sections. Arrow indicates a site of infiltration. (**D**) Lymphadenopathy (*left panels*) and absolute weight (*right panel*) of both inguinal LN. (**E**) Total number of cells extracted from both inguinal LN. (**F**) Geometric mean of FSC of live (PI^-) LN cells. Cytotoxic function of enriched lung NK cells (**G**) and of total WBC (**H**) extracted from lungs, measured as the percentage [^{51}Cr] release of killed YAC-1 tumor cells normalized to maximum [^{51}Cr] release of saponin control and corrected for spontaneous [^{51}Cr] release. (**I**) Degranulation of enriched splenic NK cells, as determined by the percentage of $PI^-CD3^-CD122^+CD49b^+$ cells positive for CD107a surface expression (*left panel*) and the geometric MFI of CD107a on positive NK cells (*right panel*). Dots represent a pool of two mice. Percentage and absolute number of NK cells in lung (**J**) and blood (**K**), gated as $CD122^+$ $CD49b^+$ cells of $CD3^-PI^-$ cells. Dots in (B), (D)–(F), (J), and (K) represent individual animals. (G) Dots represent the average of triplicate measurements from samples pooled from five to eight mice. (H) Dots represent the average of triplicate measurements for a single mouse. Horizontal bars represent median group values. Data are from one or two experiments and are representative of 2 to ≥10 independent experiments with at least four mice/experimental group. Data were obtained on day 5 p.i. $*p < 0.05$, $**p < 0.01$, $***p < 0.001$, Mann–Whitney *U* test. NI, not infected; R, red pulpa; W, white pulpa.

LN (Fig. 3K), this points toward augmented Ag presentation in MCMV-infected BALB/c mice. Histiocytes from infected BALB/c mice were substantially more activated compared with histiocytes from infected C57BL/6 mice (Supplemental Fig. 2C, 2D).

Immune cell hyperactivation in MCMV-infected BALB/c mice was accompanied by the emergence of a cytokine storm, which was evident from day 2 p.i., when type I IFN peaked in the plasma of infected mice, whereas it was undetectable in naive mice (Fig. 4A, 4B). On day 5 p.i., upregulation of mRNA expression of IFN-γ, IL-1β, IL-6, IL-18, and TNF-α, all proinflammatory cytokines classically associated with HLH (43, 51–54), was detected in cells extracted from blood, spleen, liver, and lungs (data not shown). The data were confirmed at the protein level for all mentioned cytokines, with additional elevation of IL-2 and IL-12p70 in serum (Fig. 4C–I). Notably, serum concentrations of IFN-γ were higher than those of all other cytokines and reached levels within the ng/ml range (Fig. 4C). Expression of the anti-inflammatory cytokines IL-18–binding protein and IL-10 was also upregulated at the mRNA level in blood leukocytes, spleen, liver, and lungs (data not shown). This was confirmed for IL-10 at the protein level (Fig. 4J). Proinflammatory cytokine levels in serum of infected C57BL/6 mice were elevated as well, but to a much lower extent (Supplemental Fig. 2F–L).

Hence, an increased activation status of lymphocytes and myeloid cells, together with elevated levels of multiple cytokines, characterizes the HLH-like syndrome occurring in infected WT BALB/c mice as a hyperinflammatory cytokine storm syndrome. Infected WT C57BL/6 mice presented with milder inflammation, as evidenced by less pronounced immune cell activation and lower cytokine levels compared with BALB/c mice.

$CD8^+$ T cells are dispensable in the pathogenesis of the virus-associated secondary HLH-like syndrome

Because primary HLH mouse models ascribe a major role to overactivated $CD8^+$ T cells in the development of HLH-like symptoms, the different activation status of $CD8^+$ T cells in BALB/c versus C57BL/6 mice might account for the emergence of an HLH-like syndrome in BALB/c mice only. To test this hypothesis, $CD8^+$ T cells were depleted in BALB/c mice in a preventive manner (on day −1 prior to infection) and in a therapeutic manner (on day 2 p.i., when the first disease symptoms appeared). Although adequate depletion was confirmed in LN (Supplemental

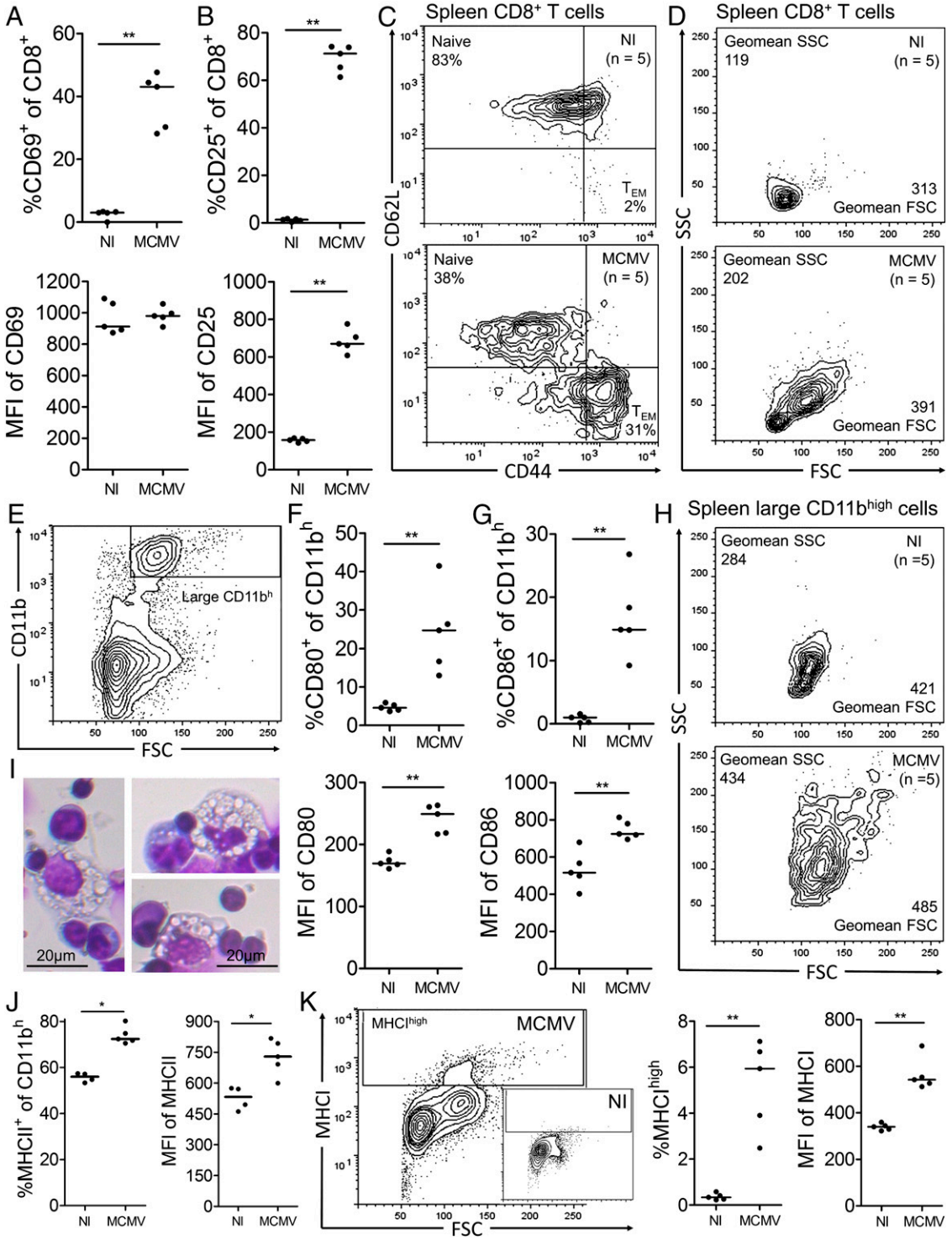

FIGURE 3. Hyperactivation of cytotoxic T cells and CD11b$^+$ cells in WT BALB/c mice infected with 5×10^3 PFU of MCMV. Expression of CD69 (**A**) and CD25 (**B**) on splenic CD8$^+$ T cells. Percentage of CD8$^+$ T cells that stain positive for CD69 or CD25 and the geometric MFI of positive cells. (**C**) Subdivision of spleen CD8$^+$ T cells into naive (CD44$^-$CD62L$^+$) and T_{EM} (CD44$^+$CD62L$^-$). Average percentages for five mice are indicated in the corresponding quadrants. (**D**) FSC and SSC plot of spleen CD8$^+$ T cells. Average geometric means for five mice are indicated. (**E**) Gating strategy to analyze large CD11b^{high} (CD11b^h) cells from spleen. Expression of CD80 (**F**) and CD86 (**G**) on splenic large CD11b^h cells. Percentage of large CD11b^h cells that stain positive for CD80 or CD86 and the geometric MFI of positive cells. (**H**) FSC and SSC plot of splenic large CD11b^{high} cells. Average geometric means for five mice are indicated. (**I**) Increased vacuolization in macrophages, as seen in H&E-stained cytospins from spleen of MCMV-infected BALB/c mice. (**J**) Expression of MHCII on large CD11b^h cells from LN. Percentage of large CD11b^h cells that stain positive for MHCII (*left panel*) and their geometric MFI of MHCII (*right panel*). (**K**) Overall expression of MHCI on splenocytes. Gating strategy to investigate MHCI^{high} cells (*left panel*). Percentage of splenocytes that stain highly positive for MHCI (*middle panel*) and their geometric MFI of MHCI (*right panel*). Dots in (A), (B), (F), (G), (J), and (K) represent a single animal. Horizontal lines represent median group values. Data are from one experiment and are representative of two to six independent experiments with at least four mice/experimental group. Data were obtained on day 5 p.i. $*p < 0.05$, $**p < 0.01$, Mann–Whitney U test. NI, not infected.

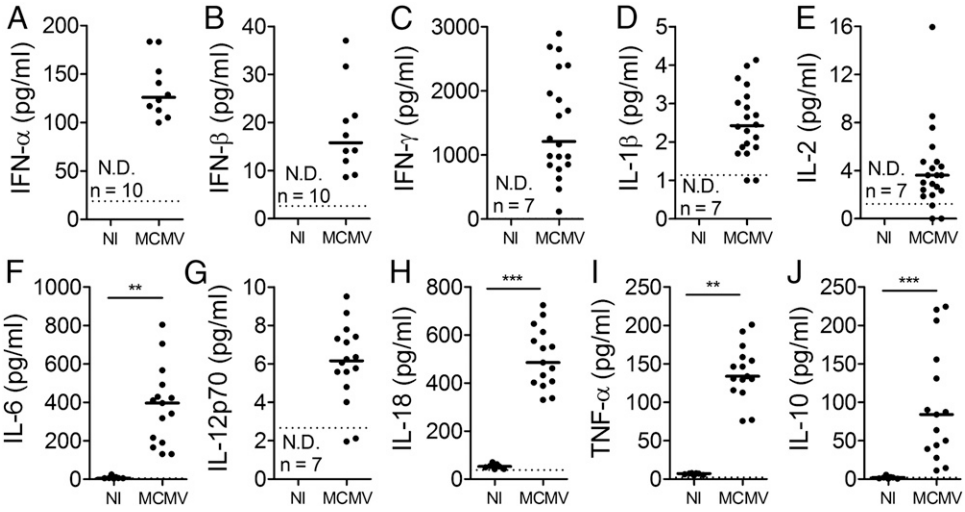

FIGURE 4. Cytokine storm in WT BALB/c mice infected with 5×10^3 PFU of MCMV. Plasma concentration (pg/ml) of IFN-α (**A**) and IFN-β (**B**) on day 2 p.i. Data were obtained via multiplex ELISA and represent two independent experiments with five mice/experimental group. Serum concentration of IFN-γ (**C**), IL-1β (**D**), IL-2 (**E**), IL-6 (**F**), IL-12p70 (**G**), IL-18 (**H**), TNF-α (**I**), and IL-10 (**J**) (pg/ml) on day 5 p.i. Data are from two independent experiments analyzed via multiplex ELISA and confirmed via single ELISA for one to four independent experiments with at least five mice/experimental group. Dots represent individual animals. Horizontal lines represent median group values. Dotted lines represent the lower detection limits of ELISA. $^{**}p < 0.01$, $^{***}p < 0.001$, Mann–Whitney *U* test. N.D., not detectable; NI, not infected.

Fig. 3A) and blood (data not shown), neither treatment succeeded in inhibiting or curing the HLH-like syndrome (Supplemental Fig. 3B–G). Only the plasma levels of sCD25 were normalized in BALB/c mice treated in a preventative manner with anti-CD8 Abs; however, this probably reflects the depletion of its cellular source rather than disease improvement (Supplemental Fig. 3F). The small, remaining population of $CD8^+$ T cells was more profoundly activated, as evident from the increased percentage of $CD69^+$ and $CD25^+$ cells, but it was unable to constrain the viral proliferation, which manifested as increased viral titers in spleen postdepletion (Supplemental Fig. 3H–J). This lack of viral control might explain the absence of any therapeutic effects.

In conclusion, the data indicate that $CD8^+$ T cells perform a redundant function in the pathogenesis of this model. As opposed to their central pathogenic role in primary HLH, $CD8^+$ T cells constitute a defensive factor in virus-associated secondary HLH.

IFN-γ is not a pathogenic cytokine in the virus-associated secondary HLH-like syndrome

In mouse models of primary HLH, a key pathogenic role is attributed to hyperproduction of IFN-γ. Because IFN-γ levels in the serum of MCMV-infected BALB/c mice were more strongly elevated than those of all other cytokines and were ~5–8-fold higher than levels observed in infected C57BL/6 mice, we sought to clarify its role in virus-associated secondary HLH by comparing disease evolution in WT and IFN-γ–KO BALB/c mice. Intriguingly, many symptoms were similar in the presence and absence of IFN-γ. Both mouse strains developed fever, lymphopenia, thrombocytopenia, anemia, hemophagocytosis, lymphadenopathy, and decreased NK cell numbers to a similar extent (Supplemental Fig. 4). Nonetheless, the syndrome progressed more rapidly in infected IFN-γ–KO mice, with increased weight loss and a higher frequency of hypothermia (in 75–85% of IFN-γ–KO mice versus 40% of WT BALB/c mice) at day 5 p.i. (Fig. 5A, 5B), indicative of increased fatality. Other symptoms were more pronounced in IFN-γ–KO mice: plasma levels of ferritin (H and L chains), sCD25, and liver enzymes (ALT and AST) were greater after viral infection in the absence of IFN-γ (Fig. 5C–E). Viral titers in spleen, lung, liver, kidney, and salivary glands were higher in IFN-γ–KO mice compared with WT mice. The difference between the mouse strains was significant from day 2 to 5 p.i. (Fig. 5F, 5G). Additionally, the accompanying cytokine storm was intensified in IFN-γ–KO mice: IL-1β, IL-6, IL-10, and TNF-α protein levels were higher in the plasma of infected mutant mice (Fig. 6A–D).

Together, these data constitute evidence that HLH-like symptoms, including anemia and hemophagocytosis, could be elicited p.i. with MCMV in the absence of IFN-γ, signifying that IFN-γ is dispensable in the pathogenesis of the HLH-like syndrome in infected BALB/c mice. Type I IFN did not appear to compensate for the lack of IFN-γ in the mutant mice, because levels of IFN-α and IFN-β were lower in infected IFN-γ–KO mice compared with infected WT BALB/c mice (Fig. 6E, 6F).

MCMV-infected IFN-γ–deficient mice develop a more complete spectrum of HLH

Additional symptoms were found exclusively in infected IFN-γ–KO mice, corresponding more closely to the clinical picture seen in HLH patients. Splenomegaly was absent in infected WT BALB/c mice of all ages, and it was not observed in IFN-γ–KO mice infected before the age of 5 wk. However, when infected at ≥5 wk of age, 80% of IFN-γ–KO mice displayed significant enlargement of the spleen (Fig. 7A). Examination of the coagulation system in infected IFN-γ–KO mice showed no hypofibrinogenemia (data not shown), but it revealed elevated plasma levels of D-dimers, a degradation product of fibrin (Fig. 7B). Elevated levels of D-dimers are indicative of disseminated intravascular coagulation (55), which is observed commonly in HLH patients (56). Further evidence for a coagulation problem in MCMV-infected IFN-γ–KO mice was found by analyzing their ability to generate thrombin (Fig. 7D). Compared with naive counterparts, MCMV-infected IFN-γ–KO mice produced less total thrombin over time and had a lower peak thrombin production. More time was required to initiate thrombin generation and to reach peak thrombin production, resulting in an overall decreased production rate. Together, the data indicated a marked reduction in their coagulation potential, which occasionally manifested as minor internal hemorrhages (inset, Fig. 7D), reflecting the bleeding diathesis of patients (56). Another feature reminiscent of HLH that is inherent to

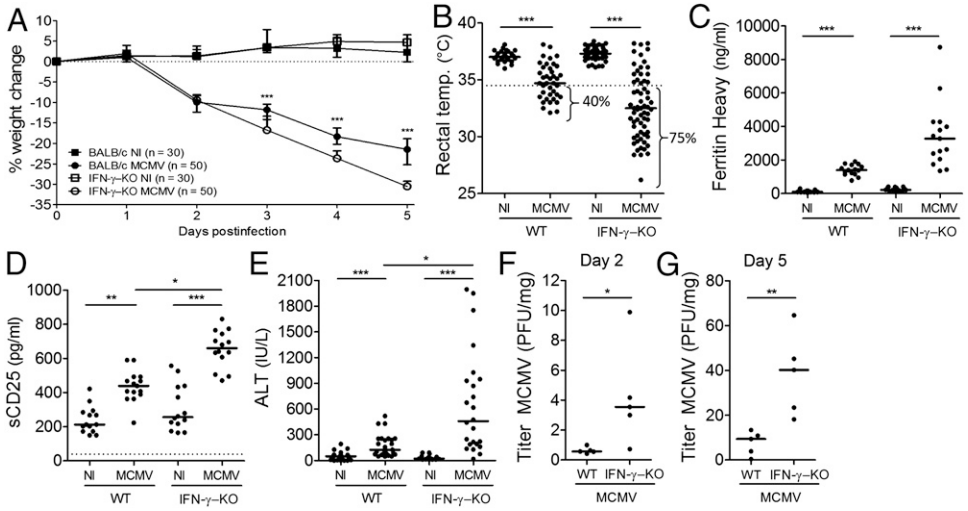

FIGURE 5. More pronounced HLH-like features in the absence of IFN-γ in BALB/c mice infected with 5×10^3 PFU of MCMV. (**A**) Percentage change in body weight relative to initial body weight at day 0 p.i. Median with interquartile range of 30 or 50 mice/experimental group. Weight change was significantly different between infected WT and IFN-γ–KO BALB/c mice on days 3–5 p.i. (***). (**B**) Rectal body temperature (˚C) on day 5 p.i. Dotted line = 34.5˚C (i.e., endpoint as an indication of mortality). (**C**) Plasma concentration of the ferritin H chain (ng/ml) on day 5 p.i. Dots represent the average of two dilutions for a single mouse. (**D**) Plasma concentration of sCD25 (pg/ml) on day 5 p.i. Dotted line represents the ELISA lower detection limit. (**E**) Plasma concentration of ALT (IU/l) on day 5 p.i. Titer of infectious virus in spleen (PFU/mg spleen tissue) at day 2 (**F**) and day 5 (**G**) p.i. Dots in (B) and (D)–(G) represent individual animals. Horizontal lines represent median group values. Data are from two to five independent experiments and are representative of a total of four to eight independent experiments with at least four mice/experimental group. *$p < 0.05$, **$p < 0.01$, ***$p < 0.001$, Kruskal–Wallis test with the Dunn posttest. NI, not infected; temp., temperature.

IFN-γ–KO mice is their reduced NK cell cytotoxic function compared with WT BALB/c mice (57). Only a minor increase in the killing capacity of NK cells was observed in IFN-γ–KO mice p.i. (Fig. 7C).

In total, the HLH-like symptoms present in MCMV-infected IFN-γ–KO mice fulfilled seven of the eight HLH-2004 diagnostic criteria, revealing a more complete spectrum of HLH in the absence of IFN-γ.

Discussion

Mouse models of primary HLH contributed greatly to our understanding of its pathogenesis. As to secondary HLH, despite the availability of various animal models, reflecting virus-associated (16), bacterial-associated (12), and autoinflammation-associated forms of the disease (13, 14), the underlying mechanisms remain poorly understood. In particular, the role of herpesvirus

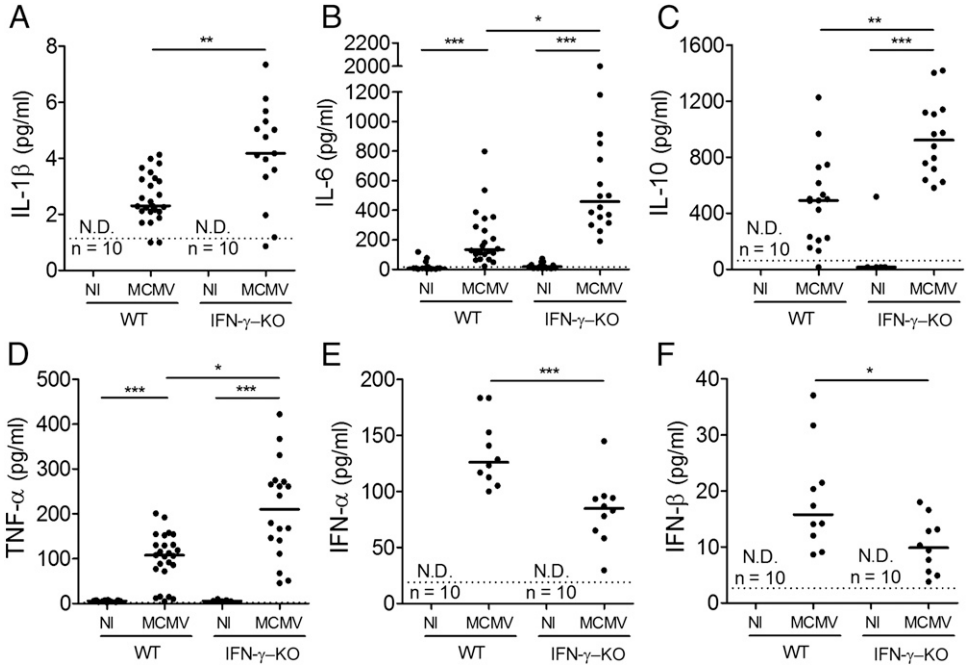

FIGURE 6. The cytokine storm is amplified in IFN-γ–KO BALB/c mice infected with 5×10^3 PFU of MCMV. Plasma concentration of IL-1β (**A**), IL-6 (**B**), IL-10 (**C**), and TNF-α (**D**) (pg/ml) on day 5 p.i., as determined via single ELISA. Serum concentration of IFN-α (**E**) and IFN-β (**F**) on day 2 p.i., determined with a multiplex ELISA. Dots represent individual animals. Horizontal lines represent median group values. Dotted lines represent the lower detection limits of ELISA. Data are from two to five independent experiments and are representative of a total of three to eight independent experiments with at least four mice/experimental group. *$p < 0.05$, **$p < 0.01$, ***$p < 0.001$, Kruskal–Wallis test with Dunn posttest. N.D., not detectable; NI, not infected.

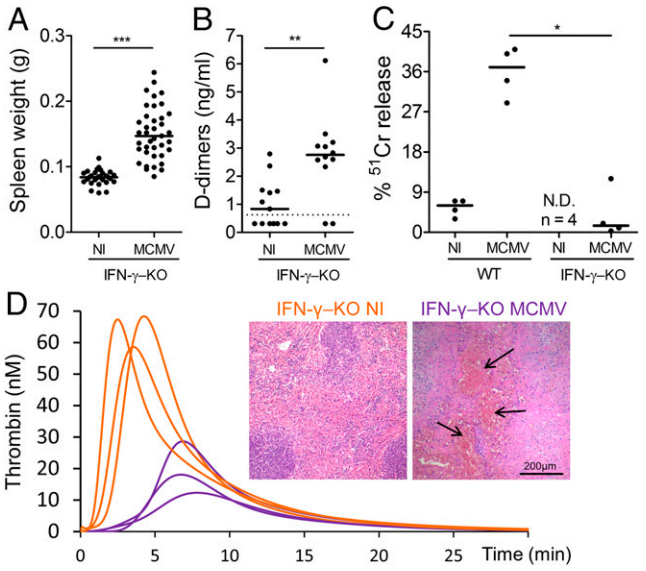

FIGURE 7. Additional HLH-like symptoms, absent in WT BALB/c mice, develop in IFN-γ–KO BALB/c mice p.i. with 5×10^3 PFU of MCMV. (**A**) Absolute spleen weight (g) of 5-wk-old IFN-γ–KO mice. Data are from seven independent experiments with at least five mice/experimental group. (**B**) Plasma concentration of D-dimers (ng/ml). Dotted line represents the lower detection limit of ELISA. Data are representative of two experiments with at least five mice/experimental group. Dots in (A) and (B) represent individual animals. (**C**) NK cell cytotoxic function of total WBC extracted from lungs, measured as the percentage of [^{51}Cr] release of killed YAC-1 tumor cells normalized to maximum [^{51}Cr] release of saponin control and corrected for spontaneous [^{51}Cr] release. Dots represent the average of triplicate measurements for a single mouse at an E:T ratio of 25:1 (confirmed at a ratio of 50:1). Data are representative of two experiments with at least four mice/experimental group. Horizontal lines represent the median group values. (**D**) Thrombin generation as a function of time measured in whole blood. The plot represents data from three mice in each group that are representative of a total of 12 mice/experimental group in two independent experiments. Inset: H&E-stained paraffin sections of spleen; arrows indicate hemorrhaging. Data were obtained on day 5 p.i. $*p < 0.05$, $**p < 0.01$, $***p < 0.001$, Mann–Whitney *U* test for a single comparison, Kruskal–Wallis test with the Dunn posttest for multiple comparisons. N.D., not detectable; NI, not infected.

infection in HLH development requires further examination, because such infection is recognized as the dominant triggering event of primary and secondary HLH episodes (21, 23, 58). The β-herpesvirus MCMV is among the most extensively studied viruses of mice, mirroring CMV infection in man (25). In the current study, we demonstrated that experimental infection of WT C57BL/6 mice with MCMV provoked a controlled and limited inflammatory response, whereas the susceptible BALB/c mouse strain developed an acute hyperinflammatory syndrome whose clinicopathological features closely resembled the life-threatening syndrome observed in HLH patients. Fever, lymphopenia, thrombocytopenia, anemia, hemophagocytosis, hyperferritinemia, elevated plasma levels of sCD25, liver dysfunction, lymphadenopathy, decreased NK cell numbers, hyperactivation of $CD8^+$ and $CD11b^+$ cells, heightened Ag presentation, and elevated levels of multiple proinflammatory cytokines were observed p.i.; all features are highly reminiscent of HLH in patients. Thus, MCMV-infected WT BALB/c mice fulfilled five of eight diagnostic criteria of the HLH-2004 protocol, supporting its validity as a new mouse model of secondary HLH.

The degree of resemblance of the HLH-like syndrome in MCMV-infected WT BALB/c mice to the clinical picture in patients with secondary HLH is similar to that of other established mouse models of secondary HLH. Typically, the syndrome is not full-blown, and only some of the HLH-2004 criteria are observed (reviewed in Ref. 17). For instance, in WT mice treated with TLR9-triggering CpG during IL-10R blockade (14) and in IL-6–transgenic mice treated with TLR4-triggering LPS (13), two models of autoinflammation-associated secondary HLH, four of eight and three of eight of the diagnostic criteria are fulfilled, respectively. Nevertheless, they provide valuable insights into the immunological mechanisms underlying the hyperinflammatory syndrome of HLH. Of note, TLR9 is also a key receptor for recognition of MCMV and EBV (59). Thus, herpesviruses might owe their HLH-triggering potential to their ability to persistently stimulate extracellular and intracellular TLRs.

Previous studies on animal models of infection-associated secondary HLH emphasized the importance of impaired pathogen clearance in the pathogenesis of HLH. In a model of bacteria-associated secondary HLH, excessive proliferation of *Salmonella* correlated with disease severity (12). In a humanized mouse model of EBV-associated secondary HLH, heat inactivation of the inoculated virus abrogated the development of the syndrome (16). These data are consistent with findings in our mouse model: persistently high infectious viral titers were present in BALB/c mice, whereas C57BL/6 mice quickly controlled the viral replication. Likewise, mouse models of primary HLH rely on persistent viral infection; the infectious agent triggering HLH cannot be cleared, despite a powerful immune response (4, 7). Reports of patients with EBV-associated HLH corroborate these findings in mouse models. EBV genome copy numbers correlate with disease severity and increase to much higher levels in EBV-associated HLH than in infectious mononucleosis (60). Out-of-control pathogen replication and persistent pathogen exposure can feed ongoing Ag presentation, prolong T cell hyperactivation, and stimulate further cytokine production, ultimately resulting in an HLH-like syndrome (7, 41, 42). In this regard, it is clear why antivirals are an important part of the supportive measures used in the HLH-2004 therapeutic protocol for patients with primary and secondary HLH (32). In both subtypes it is critical to search for and eliminate any triggering agents, to terminate the ongoing immune stimulation (56). However, removal of the pathogen alone is usually insufficient to cure full-blown HLH. In patients with virus-associated secondary HLH, monotherapy with antivirals is often inadequate to obtain complete remission (20, 21, 23). Antivirals can help to prevent and treat HLH, but ideally, a combination with immunosuppressive drugs should be considered to halt virus- and immune-mediated pathology.

In primary HLH, hypersecretion of IFN-γ by aberrantly activated $CD8^+$ T cells is assumed to be the main cause of immunopathology (4, 10), directly mediating hemophagocytosis and cytopenias (11). However, in our model, neither $CD8^+$ T cells nor IFN-γ played a similar pathogenic role. Development and progression of the HLH-like syndrome was undiminished following $CD8^+$ T cell depletion, as well as in IFN-γ–deficient mice, complete with hemophagocytosis and cytopenias. Moreover, IFN-γ–deficient mice showed a worse prognosis, with aggravated hyperferritinemia, more highly elevated sCD25 levels, worsened liver dysfunction, and an intensified cytokine storm. Additional HLH symptoms appeared in the absence of IFN-γ, including splenomegaly, coagulopathy, and decreased NK cell cytotoxicity. Thus, in virus-associated secondary HLH, IFN-γ appears to play a role entirely different from that in primary HLH. Through its potent direct antiviral effect and NK cell–stimulating function (61), the cytokine may exert a protective role in virus-associated secondary HLH. Because we found higher viral titers in infected IFN-γ–KO mice versus WT counterparts, it is tempting to speculate that the more severe HLH-like disease in these mutant mice is a direct

result of the absence of IFN-γ as an antiviral protein. However, the additional HLH symptoms that were found exclusively in IFN-γ–KO mice did not correlate with spleen viral titers and were not observed in WT BALB/c mice challenged with a dose of MCMV that was 2, 5, or even 25 times higher (data not shown). Therefore, it is unlikely that the HLH phenotype of infected IFN-γ–KO mice is a result of the lack of the antiviral activity of IFN-γ; rather, it may be ascribed to the loss of its immunomodulatory effects on, for instance, neutrophil-mediated pathologies (62). Our observations with respect to the HLH mouse model in the absence of IFN-γ are of clinical relevance because, recently, a first report appeared on two IFN-γR–deficient patients who acquired HLH after herpesvirus and mycobacterial infection (63). In these patients, the syndrome must have developed in an IFN-γ–independent way, arguing against the existence of a general pathogenic pathway that would cause both primary and secondary HLH (19, 64). Alternative pathways, also IFN-γ–independent ones (13, 18, 65), are capable of inducing a similar syndrome. Therefore, caution should be exercised when extrapolating treatment options from primary to secondary HLH (19). Specifically, the use of anti–IFN-γ Ab in secondary HLH may not be beneficial. In secondary HLH, attention should be given to therapeutic strategies that limit immunopathology while maintaining antipathogen immunity.

Acknowledgments

We thank Dr. Joke Konings and Dr. Evelien Schurgers for assistance during the coagulation experiments and Prof. Alfons Billiau for critical revision of the manuscript.

Disclosures

The authors have no financial conflicts of interest.

References

1. Janka, G. E. 2007. Familial and acquired hemophagocytic lymphohistiocytosis. *Eur. J. Pediatr.* 166: 95–109.
2. Janka, G. E., and K. Lehmberg. 2013. Hemophagocytic lymphohistiocytosis: pathogenesis and treatment. *Hematology Am. Soc. Hematol. Educ. Program* 2013: 605–611.
3. Walsh, C. M., M. Matloubian, C. C. Liu, R. Ueda, C. G. Kurahara, J. L. Christensen, M. T. Huang, J. D. Young, R. Ahmed, and W. R. Clark. 1994. Immune function in mice lacking the perforin gene. *Proc. Natl. Acad. Sci. USA* 91: 10854–10858.
4. Jordan, M. B., D. Hildeman, J. Kappler, and P. Marrack. 2004. An animal model of hemophagocytic lymphohistiocytosis (HLH): CD8+ T cells and interferon gamma are essential for the disorder. *Blood* 104: 735–743.
5. Kögl, T., J. Müller, B. Jessen, A. Schmitt-Graeff, G. Janka, S. Ehl, U. zur Stadt, and P. Aichele. 2013. Hemophagocytic lymphohistiocytosis in syntaxin-11-deficient mice: T-cell exhaustion limits fatal disease. *Blood* 121: 604–613.
6. D'Orlando, O., F. Zhao, B. Kasper, Z. Orinska, J. Müller, I. Hermans-Borgmeyer, G. M. Griffiths, U. Zur Stadt, and S. Bulfone-Paus. 2013. Syntaxin 11 is required for NK and $CD8^+$ T-cell cytotoxicity and neutrophil degranulation. *Eur. J. Immunol.* 43: 194–208.
7. Crozat, K., K. Hoebe, S. Ugolini, N. A. Hong, E. Janssen, S. Rutschmann, S. Mudd, S. Sovath, E. Vivier, and B. Beutler. 2007. Jinx, an MCMV susceptibility phenotype caused by disruption of Unc13d: a mouse model of type 3 familial hemophagocytic lymphohistiocytosis. *J. Exp. Med.* 204: 853–863.
8. Pachlopnik Schmid, J., C.-H. Ho, J. Diana, G. Pivert, A. Lehuen, F. Geissmann, A. Fischer, and G. de Saint Basile. 2008. A Griscelli syndrome type 2 murine model of hemophagocytic lymphohistiocytosis (HLH). *Eur. J. Immunol.* 38: 3219–3225.
9. Jessen, B., A. Maul-Pavicic, H. Ufheil, T. Vraetz, A. Enders, K. Lehmberg, A. Längler, U. Gross-Wieltsch, A. Bay, Z. Kaya, et al. 2011. Subtle differences in CTL cytotoxicity determine susceptibility to hemophagocytic lymphohistiocytosis in mice and humans with Chediak-Higashi syndrome. *Blood* 118: 4620–4629.
10. Pachlopnik Schmid, J., C.-H. Ho, F. Chrétien, J. M. Lefebvre, G. Pivert, M. Kosco-Vilbois, W. Ferlin, F. Geissmann, A. Fischer, and G. de Saint Basile. 2009. Neutralization of IFNgamma defeats haemophagocytosis in LCMV-infected perforin- and Rab27a-deficient mice. *EMBO Mol. Med.* 1: 112–124.
11. Zoller, E. E., J. E. Lykens, C. E. Terrell, J. Aliberti, A. H. Filipovich, P. M. Henson, and M. B. Jordan. 2011. Hemophagocytosis causes a consumptive anemia of inflammation. *J. Exp. Med.* 208: 1203–1214.
12. Brown, D. E., M. W. McCoy, M. C. Pilonieta, R. N. Nix, and C. S. Detweiler. 2010. Chronic murine typhoid fever is a natural model of secondary hemophagocytic lymphohistiocytosis. *PLoS One* 5: e9441.
13. Strippoli, R., F. Carvello, R. Scianaro, L. De Pasquale, M. Vivarelli, S. Petrini, L. Bracci-Laudiero, and F. De Benedetti. 2012. Amplification of the response to Toll-like receptor ligands by prolonged exposure to interleukin-6 in mice: implication for the pathogenesis of macrophage activation syndrome. *Arthritis Rheum.* 64: 1680–1688.
14. Behrens, E. M., S. W. Canna, K. Slade, S. Rao, P. A. Kreiger, M. Paessler, T. Kambayashi, and G. A. Koretzky. 2011. Repeated TLR9 stimulation results in macrophage activation syndrome-like disease in mice. *J. Clin. Invest.* 121: 2264–2277.
15. Hayashi, K., N. Ohara, N. Teramoto, S. Onoda, H. L. Chen, T. Oka, E. Kondo, T. Yoshino, K. Takahashi, J. Yates, and T. Akagi. 2001. An animal model for human EBV-associated hemophagocytic syndrome: herpesvirus papio frequently induces fatal lymphoproliferative disorders with hemophagocytic syndrome in rabbits. *Am. J. Pathol.* 158: 1533–1542.
16. Sato, K., N. Misawa, C. Nie, Y. Satou, D. Iwakiri, M. Matsuoka, R. Takahashi, K. Kuzushima, M. Ito, K. Takada, and Y. Koyanagi. 2011. A novel animal model of Epstein-Barr virus-associated hemophagocytic lymphohistiocytosis in humanized mice. *Blood* 117: 5663–5673.
17. Brisse, E., C. H. Wouters, and P. Matthys. 2015. Hemophagocytic lymphohistiocytosis (HLH): A heterogeneous spectrum of cytokine-driven immune disorders. *Cytokine Growth Factor Rev.* 26: 263–280.
18. Canna, S. W., J. Wrobel, N. Chu, P. A. Kreiger, M. Paessler, and E. M. Behrens. 2013. Interferon-γ mediates anemia but is dispensable for fulminant toll-like receptor 9-induced macrophage activation syndrome and hemophagocytosis in mice. *Arthritis Rheum.* 65: 1764–1775.
19. Canna, S. W., and E. M. Behrens. 2012. Not all hemophagocytes are created equally: appreciating the heterogeneity of the hemophagocytic syndromes. *Curr. Opin. Rheumatol.* 24: 113–118.
20. Maakaroun, N. R., A. Moanna, J. T. Jacob, and H. Albrecht. 2010. Viral infections associated with haemophagocytic syndrome. *Rev. Med. Virol.* 20: 93–105.
21. Rouphael, N. G., N. J. Talati, C. Vaughan, K. Cunningham, R. Moreira, and C. Gould. 2007. Infections associated with haemophagocytic syndrome. *Lancet Infect. Dis.* 7: 814–822.
22. Ansuini, V., D. Rigante, and S. Esposito. 2013. Debate around infection-dependent hemophagocytic syndrome in paediatrics. *BMC Infect. Dis.* 13: 15.
23. Ramos-Casals, M., P. Brito-Zerón, A. López-Guillermo, M. A. Khamashta, and X. Bosch. 2014. Adult haemophagocytic syndrome. *Lancet* 383: 1503–1516.
24. van Dommelen, S. L. H., N. Sumaria, R. D. Schreiber, A. A. Scalzo, M. J. Smyth, and M. A. Degli-Esposti. 2006. Perforin and granzymes have distinct roles in defensive immunity and immunopathology. *Immunity* 25: 835–848.
25. Krmpotic, A., I. Bubic, B. Polic, P. Lucin, and S. Jonjic. 2003. Pathogenesis of murine cytomegalovirus infection. *Microbes Infect.* 5: 1263–1277.
26. Corbett, A. J., J. D. Coudert, C. A. Forbes, and A. A. Scalzo. 2011. Functional consequences of natural sequence variation of murine cytomegalovirus m157 for Ly49 receptor specificity and NK cell activation. *J. Immunol.* 186: 1713–1722.
27. Tagawa, Y., K. Sekikawa, and Y. Iwakura. 1997. Suppression of concanavalin A-induced hepatitis in IFN-gamma(−/−) mice, but not in TNF-alpha(−/−) mice: role for IFN-gamma in activating apoptosis of hepatocytes. *J. Immunol.* 159: 1418–1428.
28. Ninivaggi, M., H. Kelchtermans, M. J. Kuijpers, B. Hemmeryckx, J. W. M. Heemskerk, T. Lindhout, M. F. Hoylaerts, and B. de Laat. 2014. Whole blood thrombin generation in Bmal1-deficient mice. *Thromb. Haemost.* 112: 271–275.
29. Billiau, A. D., H. Sefrioui, L. Overbergh, O. Rutgeerts, J. Goebels, C. Mathieu, and M. Waer. 2001. Transforming growth factor-beta inhibits lymphokine activated killer cytotoxicity of bone marrow cells: implications for the graft-versus-leukemia effect in irradiation allogeneic bone marrow chimeras. *Transplantation* 71: 292–299.
30. Livak, K. J., and T. D. Schmittgen. 2001. Analysis of relative gene expression data using real-time quantitative PCR and the 2(-Delta Delta C(T)) Method. *Methods* 25: 402–408.
31. Santambrogio, P., A. Cozzi, S. Levi, E. Rovida, F. Magni, A. Albertini, and P. Arosio. 2000. Functional and immunological analysis of recombinant mouse H- and L-ferritins from *Escherichia coli*. *Protein Expr. Purif.* 19: 212–218.
32. Henter, J. I., A. Horne, M. Arico, R. M. Egeler, D. Webb, J. Winiarski, and G. Janka. 2007. HLH-2004 : Diagnostic and therapeutic guidelines for hemophagocytic lymphohistiocytosis. *Pedriatr. Blood Cancer* 48: 124–131.
33. Chan, C. B., M. Abe, N. Hashimoto, C. Hao, I. R. Williams, X. Liu, S. Nakao, A. Yamamoto, C. Zheng, J. I. Henter, et al. 2009. Mice lacking asparaginyl endopeptidase develop disorders resembling hemophagocytic syndrome. *Proc. Natl. Acad. Sci. USA* 106: 468–473.
34. Green, R. M., and S. Flamm. 2002. AGA technical review on the evaluation of liver chemistry tests. *Gastroenterology* 123: 1367–1384.
35. Bryceson, Y. T., D. Pende, A. Maul-Pavicic, K. C. Gilmour, H. Ufheil, T. Vraetz, S. C. Chiang, S. Marcenaro, R. Meazza, I. Bondzio, et al. 2012. A prospective evaluation of degranulation assays in the rapid diagnosis of familial hemophagocytic syndromes. *Blood* 119: 2754–2763.
36. Aricò, M., M. Allen, S. Brusa, R. Clementi, D. Pende, R. Maccario, L. Moretta, and C. Danesino. 2002. Haemophagocytic lymphohistiocytosis: proposal of a diagnostic algorithm based on perforin expression. *Br. J. Haematol.* 119: 180–188.
37. Grom, A. A., J. Villanueva, S. Lee, E. A. Goldmuntz, M. H. Passo, and A. Filipovich. 2003. Natural killer cell dysfunction in patients with systemic-onset juvenile rheumatoid arthritis and macrophage activation syndrome. *J. Pediatr.* 142: 292–296.

38. Alter, G., J. M. Malenfant, and M. Altfeld. 2004. CD107a as a functional marker for the identification of natural killer cell activity. *J. Immunol. Methods* 294: 15–22.
39. Grom, A. A. 2004. Natural killer cell dysfunction: A common pathway in systemic-onset juvenile rheumatoid arthritis, macrophage activation syndrome, and hemophagocytic lymphohistiocytosis? *Arthritis Rheum.* 50: 689–698.
40. Kogawa, K., S. M. Lee, J. Villanueva, D. Marmer, J. Sumegi, and A. H. Filipovich. 2002. Perforin expression in cytotoxic lymphocytes from patients with hemophagocytic lymphohistiocytosis and their family members. *Blood* 99: 61–66.
41. Terrell, C. E., and M. B. Jordan. 2013. Perforin deficiency impairs a critical immunoregulatory loop involving murine CD8(+) T cells and dendritic cells. *Blood* 121: 5184–5191.
42. Lykens, J. E., C. E. Terrell, E. E. Zoller, K. Risma, and M. B. Jordan. 2011. Perforin is a critical physiologic regulator of T-cell activation. *Blood* 118: 618–626.
43. Usmani, G. N., B. A. Woda, and P. E. Newburger. 2013. Advances in understanding the pathogenesis of HLH. *Br. J. Haematol.* 161: 609–622.
44. Lambotte, O., P. Cacoub, N. Costedoat, G. Le Moel, Z. Amoura, and J.-C. Piette. 2003. High ferritin and low glycosylated ferritin may also be a marker of excessive macrophage activation. *J. Rheumatol.* 30: 1027–1028.
45. Grom, A. A., and E. D. Mellins. 2010. Macrophage activation syndrome: advances towards understanding pathogenesis. *Curr. Opin. Rheumatol.* 22: 561–566.
46. Rosário, C., G. Zandman-Goddard, E. G. Meyron-Holtz, D. P. D'Cruz, and Y. Shoenfeld. 2013. The hyperferritinemic syndrome: macrophage activation syndrome, Still's disease, septic shock and catastrophic antiphospholipid syndrome. *BMC Med.* 11: 185.
47. Reddy, M., E. Eirikis, C. Davis, H. M. Davis, and U. Prabhakar. 2004. Comparative analysis of lymphocyte activation marker expression and cytokine secretion profile in stimulated human peripheral blood mononuclear cell cultures: an in vitro model to monitor cellular immune function. *J. Immunol. Methods* 293: 127–142.
48. Rea, I. M., S. E. McNerlan, and H. D. Alexander. 1999. CD69, CD25, and HLA-DR activation antigen expression on CD3+ lymphocytes and relationship to serum TNF-alpha, IFN-gamma, and sIL-2R levels in aging. *Exp. Gerontol.* 34: 79–93.
49. Kaech, S. M., S. Hemby, E. Kersh, and R. Ahmed. 2002. Molecular and functional profiling of memory CD8 T cell differentiation. *Cell* 111: 837–851.
50. Lanier, L. L., S. O'Fallon, C. Somoza, J. H. Phillips, P. S. Linsley, K. Okumura, D. Ito, and M. Azuma. 1995. CD80 (B7) and CD86 (B70) provide similar costimulatory signals for T cell proliferation, cytokine production, and generation of CTL. *J. Immunol.* 154: 97–105.
51. Mazodier, K., V. Marin, D. Novick, C. Farnarier, S. Robitail, N. Schleinitz, V. Veit, P. Paul, M. Rubinstein, C. A. Dinarello, et al. 2005. Severe imbalance of IL-18/IL-18BP in patients with secondary hemophagocytic syndrome. *Blood* 106: 3483–3489.
52. Osugi, Y., J. Hara, S. Tagawa, K. Takai, G. Hosoi, Y. Matsuda, H. Ohta, H. Fujisaki, M. Kobayashi, N. Sakata, et al. 1997. Cytokine production regulating Th1 and Th2 cytokines in hemophagocytic lymphohistiocytosis. *Blood* 89: 4100–4103.
53. Fujiwara, F., S. Hibi, and S. Imashuku. 1993. Hypercytokinemia in hemophagocytic syndrome. *Am. J. Pediatr. Hematol. Oncol.* 15: 92–98.
54. Billiau, A. D., T. Roskams, R. Van Damme-Lombaerts, P. Matthys, and C. Wouters. 2005. Macrophage activation syndrome: characteristic findings on liver biopsy illustrating the key role of activated, IFN-gamma-producing lymphocytes and IL-6- and TNF-alpha-producing macrophages. *Blood* 105: 1648–1651.
55. Carr, J. M., M. McKinney, and J. McDonagh. 1989. Diagnosis of disseminated intravascular coagulation. Role of D-dimer. *Am. J. Clin. Pathol.* 91: 280–287.
56. Jordan, M. B., C. E. Allen, S. Weitzman, A. H. Filipovich, and K. L. McClain. 2011. How I treat hemophagocytic lymphohistiocytosis. *Blood* 118: 4041–4052.
57. Dalton, D., S. Pitts-Meek, S. Keshav, I. Figari, A. Bradley, and T. Stewart. 1993. Multiple defects of immune cell function in mice with disrupted interferon-gamma genes. *Science* 259: 1739–1742.
58. Henter, J.-I., A. Ehrnst, J. Andersson, and G. Elinder. 1993. Familial hemophagocytic lymphohistiocytosis and viral infections. *Acta Paediatr.* 82: 369–372.
59. Tabeta, K., P. Georgel, E. Janssen, X. Du, K. Hoebe, K. Crozat, S. Mudd, L. Shamel, S. Sovath, J. Goode, et al. 2004. Toll-like receptors 9 and 3 as essential components of innate immune defense against mouse cytomegalovirus infection. *Proc. Natl. Acad. Sci. USA* 101: 3516–3521.
60. Teramura, T., Y. Tabata, T. Yagi, A. Morimoto, S. Hibi, and S. Imashuku. 2002. Quantitative analysis of cell-free Epstein-Barr virus genome copy number in patients with EBV-associated hemophagocytic lymphohistiocytosis. *Leuk. Lymphoma* 43: 173–179.
61. Commins, S. P., L. Borish, and J. W. Steinke. 2010. Immunologic messenger molecules: cytokines, interferons, and chemokines. *J. Allergy Clin. Immunol.* 125(2, Suppl. 2)S53–S72.
62. Kelchtermans, H., A. Billiau, and P. Matthys. 2008. How interferon-gamma keeps autoimmune diseases in check. *Trends Immunol.* 29: 479–486.
63. Tesi, B., E. Sieni, C. Neves, F. Romano, V. Cetica, A. I. Cordeiro, S. Chiang, H. Schlums, L. Galli, S. Avenali, et al. 2015. Hemophagocytic lymphohistiocytosis in 2 patients with underlying IFN-γ receptor deficiency. *J. Allergy Clin. Immunol.* 135: 1638–1641.
64. Yasumi, T., M. Hori, E. Hiejima, H. Shibata, K. Izawa, H. Oda, K. Yoshioka, K. Nakagawa, T. Kawai, R. Nishikomori, et al. 2015. Laboratory parameters identify familial haemophagocytic lymphohistiocytosis from other forms of paediatric haemophagocytosis. *Br. J. Haematol.* 170: 532–538.
65. Krebs, P., K. Crozat, D. Popkin, M. B. Oldstone, and B. Beutler. 2011. Disruption of MyD88 signaling suppresses hemophagocytic lymphohistiocytosis in mice. *Blood* 117: 6582–6588.